ADVANCED MATERIALS

the average dielectric constant is $\langle\varepsilon\rangle$ = 1.94, and increases to $\langle\varepsilon\rangle$ = 2.22 in the infiltrated one (reducing the contrast at the same time). After inversion the mean dielectric constant decreases to $\langle\varepsilon\rangle$ = 1.41 and, accordingly, the *L* pseudogap energy shifts upwards (see Fig. 5).

The peak width is a function of both the dielectric contrast and the filling factor of the structure. Bare opals present a contrast $\varepsilon_{SiO_2}/\varepsilon_{air}$ = 2.1 that shifts to $\varepsilon_{polymer}/\varepsilon_{SiO_2}$ = 1.24 when infiltration takes place. So, the pseudogap width is largely decreased, as is observed in both the experiment and band structure calculation. When inversion occurs, the dielectric contrast is increased up to $\varepsilon_{polymer}/\varepsilon_{air}$ = 2.6. It has to be noticed that, although bare and inverse opal have similar values of the refractive index contrast, inverse opals show a much broader pseudogap than the direct opal structure which reflects the fact that inverse structures are more powerful scatterers (see Fig. 5A).

When the sample is tilted with respect to normal incidence, the ***k*** vector ceases to be collinear with *Γ*–*L*. For a given direction (tilt angle), at some point of the energy scan, ***k*** crosses the Bragg plane and a reflection is obtained. Since *L* is the closest (to *Γ*) point of the Bragg plane, tilting increases both the wavevector length and the energy for which reflection occurs. This pseudogap energy position, can be followed along the *L*–*U* (or *L*–*K* or *L*–*W*) line in the Brillouin zone. In Figure 5C experimental data are superimposed on the band structure diagram by using Snell's law with an average refractive index for calculating the internal angle (with respect to the *Γ*–*L* direction). The theory gives a good account of the behavior of the pseudogap position.

In summary, we have obtained and optically analyzed polymer inverse opals with a long-range order. Their photonic crystal behavior has been studied both experimentally and theoretically, and a good agreement between band-structure calculations and experiments was found. From a fundamental point of view, they can be regarded as model systems, where studying the effect of topology and dielectric contrast is possible. Regarding their potential applications, they can be used to modify the emission properties of luminescent species, such as dyes, that can easily be incorporated into the polymer. Polymer inverse opals offer, in turn, the interesting possibility of being used as matrices to obtain new spherical colloidal particles, whose shape cannot be controlled otherwise, from different materials.

Experimental

The polymer used for infiltration was obtained by the polymerization of 15 cm^3 of an epoxy resin (Bisphenol A-epichlorhydrine, Struers) in the presence of 2 cm^3 of catalyzer (Triethylentetramin, Struers). In this way a viscous fluid is obtained in which the opal is immersed. The liquid soaks the opal and when the diffusion is completed the opal turns transparent as a consequence of the partial-index matching between silica and polymer. In about 12 h polymerization completes and the shrinkage between the liquid and the solid is less than 5 %. This allows a good filling and a very good connection of the infiltrated material. The polymer refractive index was measured by the prism minimum deviation angle and resulted to be n = 1.609 ± 0.005.

Once the infiltrated polymer has solidified, the block is cut and polished until the original outer facet of the opal is brought to the surface of the block. The same is done on the rear surface to finally obtain a sample about 200 μm thick. The polishing is carried out with alumina powder down to 0.05 μm roughness.

Received: October 5, 2000

[1] J. D. Joannopoulos, R. D. Meade, J. N. Winn, *Photonic Crystals*, Princeton University Press, Princeton, NJ **1995**.
[2] J. D. Joannopoulos, P. R. Villeneuve, S. Fan, *Nature* **1997**, *386*, 143.
[3] R. Mayoral, J. Requena, S. J. Moya, C. López, A. Cintas, H. Míguez, F. Meseguer, L. Vázquez, M. Holgado, A. Blanco, *Adv. Mater.* **1997**, *9*, 257.
[4] Y. A. Vlasov, V. N. Astratov, O. Z. Karimov, A. A. Kaplyanskii, V. N. Bogomolov, A. V. Prokofiev, *Phys. Rev. B* **1997**, *55*, 13 357.
[5] H. Míguez, C. López, F. Meseguer, A. Blanco, L. Vázquez, R. Mayoral, M. Ocaña, A. Mifsud, V. Fornés, *Appl. Phys. Lett.* **1997**, *71*, 1148.
[6] S. H. Park, Y. Xia, *Adv. Mater.* **1998**, *10*, 1045.
[7] S. A. Johnson, P. J. Oliver, T. E. Mallouk, *Science* **1999**, *283*, 963.
[8] K. Yoshino, S. B. Lee, S. Tatsuhara, Y. Kawagishi, M. Ozaki, A. A. Zakhidov, *Jpn. J. Appl. Phys. 2* **1999**, *38*, L786.
[9] K. Yoshino, S. B. Lee, S. Tatsuhara, Y. Kawagishi, M. Ozaki, A. A. Zakhidov, *Appl. Phys. Lett.* **1999**, *73*, 3506.
[10] J. F. Bertone, P. Jiang, K. S. Hwang, D. M. Mittleman, V. Colvin, *Phys. Rev. Lett.* **1999**, *83*, 300.
[11] C. López, H. Míguez, F. Meseguer, R. Mayoral, L. Vázquez, M. Ocaña, *Superlattices Microstruct.* **1997**, *22*, 399. H. Míguez, F. Meseguer C. López, A. Mifsud, J. S. Moya, L. Vázquez, *Langmuir* **1997**, *13*, 6009.
[12] G. H. Bogush, M. A. Tracy, C. F. Zukoski. *J. Non-Cryst. Solids* **1988**, *104*, 95.
[13] H. Míguez, F. Meseguer, C. López, A. Blanco, J. S. Moya, J. Requena, A. Mifsud, V. Fornés, *Adv. Mater.* **1998**, *10*, 480.
[14] E. Matijevic, *Langmuir* **1994**, *10*, 8.
[15] R. Meade, A. M. Rappe, K. D. Rommer, J. D. Joannopoulos, *Phys. Rev. B* **1993**, *48*, 8434. Erratum by S. G. Johnson, *Phys. Rev. B* **1997**, *55*, 15 942.

Structured Metallic Films for Optical and Spectroscopic Applications via Colloidal Crystal Templating**

By *Peter M. Tessier*, *Orlin D. Velev*,* *Anand T. Kalambur*, *Abraham M. Lenhoff*, *John F. Rabolt*, and *Eric W. Kaler*

Porous metallic films are promising structures for applications in photonic materials, sensors, catalysts, and energy-harvesting coatings. Here we describe how e-beam and other complex microfabrication techniques for forming such films can be replaced by a simple wet-chemistry templating method. The pores are templated by two-dimensional (2D) crystals of latex microspheres embedded into a structure assembled from gold nanoparticles. The porous metallic films formed by this method have interesting optical properties and are excellent substrates for surface-enhanced Raman spectroscopy (SERS).

[*] Prof. O. D. Velev, P. M. Tessier, Prof. A. M. Lenhoff, Prof. E. W. Kaler
Center for Molecular and Engineering Thermodynamics
Department of Chemical Engineering
University of Delaware
Newark, DE 19716 (USA)
E-mail: Velev@che.udel.edu
A. T. Kalambur, Prof. J. F. Rabolt
Department of Materials Science and Engineering
University of Delaware
Newark, DE 19716 (USA)

[**] We thank Yonghui Yuan and Rajesh Pazhianur for their help with AFM imaging and George Watson for helpful discussions.

  0935-9648/01/0603-0396 $ 17.50+.50/0

Microfabrication techniques such as e-beam lithography can be used to create porous metallic films that are sub-micrometer in both thickness and pore size. These techniques, however, have the significant limitations of being both expensive and time-consuming. An attractive alternative is based on the use of colloidal crystals of sub-micrometer latex or silica spheres as templates. The formation of structured three-dimensionally (3D) porous metals using colloidal crystal templates was reported recently by a number of groups. A metallic structure can be grown in the pores of the crystal by chemical[1] or electrochemical[2] means and the resulting material can be easily isolated by subsequent removal of the template. We have shown that 3D porous metallic structures can also be assembled from gold nanoparticles.[3] The resulting hierarchical porosity gives these materials high surface area, which is particularly important for applications such as sensing and catalysis. Nevertheless, all of these 3D metallic structures are of little practical use for optical applications, since they cannot be easily obtained as homogeneous thin films immobilized on a convenient substrate. They are also all created by multi-step procedures whereby the colloidal crystals are assembled first and the metal is then infiltrated into the voids.

In this communication we report two new methods for forming thin porous metallic films by directly coating a substrate with a mixture of latex and gold particles, which upon drying forms an ordered gold structure templated by the colloidal crystal. Conceptually, our procedures of "outside-in" templating of the overall shape by restricting and crystallizing the components within a film can be viewed as complementary to the "inside-out" templating of the internal structure of the material by the colloidal crystal.

The first step in the assembly process is the crystallization of the much larger latex particles into multilayer 2D crystals. Two alternative methods for forming such films were developed. In the first method (Fig. 1a), the films were produced by first dispensing a mixture of gold and latex particles in the angle between two glass slides. As the top slide was translated by an electric motor, the meniscus was dragged along the bottom plate and deposited a thin film of gold and latex particles, which dried at ambient conditions within 1 h.

In the second method (Fig. 1b), a static cell for the radial deposition of latex/gold films was used that was similar to that used earlier in the study of 2D particle crystallization.[4] When a mixture of gold and latex particles was placed in the circular cell chamber, a concave meniscus formed. The crystal nucleated in the center of the chamber when the wetting film was a few latex particles thick. The crystal front grew radially outward, completely filling the chamber in approximately 4 h.

Figure 1c illustrates the likely course of development of the material structure in the crystallizing region of both Figure 1a (trailing edge) and b (center). In both methods, the latex particles are ordered into a multilayer 2D crystal by a combination of an increase in the particle volume fraction in the film and convective assembly.[4,5] As the concentration of the particles in the film increases due to evaporation, the latex particles, whose volume fraction is higher, crystallize first. The

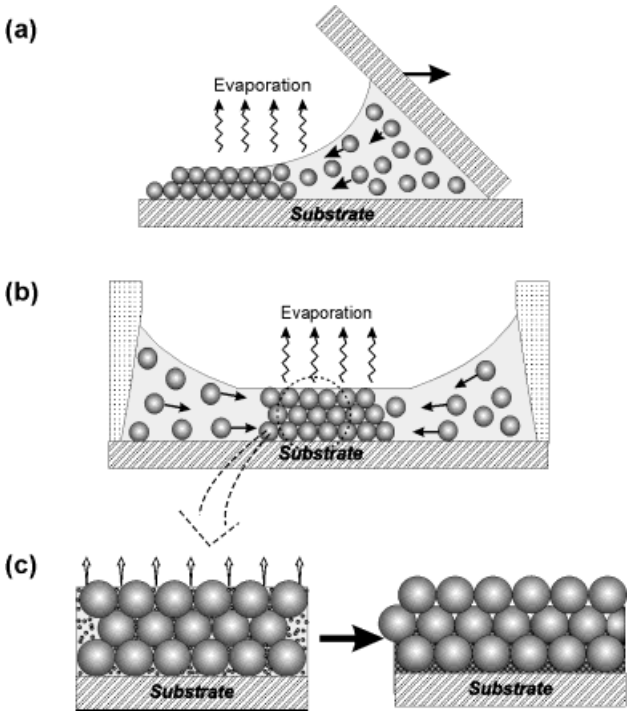

Fig. 1. Schematic diagrams of the formation of structured gold films by the template-directed assembly of gold particles by colloidal crystals. a) Directional deposition of a latex/gold crystal at the trailing edge of a moving meniscus. b) Radial growth of a latex/gold crystal in an enclosed cell. c) Enlarged view of the crystallizing region in (a) and (b) where the gold particles are concentrated at the drying front and consequently compacted due to solvent evaporation.

crystallization is enhanced by the convective flux of water, which collects the latex microspheres at the trailing edge (Fig. 1a) or center (Fig. 1b) of the meniscus. The volume fraction of the gold particles at the beginning of the process is still below their crystallization threshold. As the evaporation continues, the gold nanoparticles are concentrated at the drying front and pack together, forming a solid network around the latex microspheres (Fig. 1c).

For both assembly methods the polymer microspheres in the dried structure were dissolved by immersing the samples in toluene. The thickness of the deposited film and the resulting gold structure were controlled by the concentration of latex and the speed of deposition. For example, to form multilayer gold structures by the directional method (Fig. 1a), the required latex concentration after dilution with the gold colloid was approximately 10 vol.-% deposited at a speed of approximately 2 μm/s. At higher speeds of deposition (> ca. 10 μm/s) and lower latex volume fractions (< ca. 5 %) 2D crystals grew that yielded sub-monolayer gold structures.

A comparison of the materials obtained by the two methods showed that the quality of the long-range ordering and the homogeneity of the sample thickness were better with the directional deposition method (Fig. 1a), and the images and spectra shown herein were obtained with samples formed by this method. However, the radial deposition method has the advantage of being simpler and not using any additional equipment. It is also amenable to templating of the overall

  0935-9648/01/0603-0397 $ 17.50+.50/0

ADVANCED MATERIALS

shape of the supported patch, which cannot be accomplished readily by the other procedure.

The appearance of the resulting gold films ranged from translucent to opaque, depending on the thickness, and showed striking colors by diffraction due to the long-range ordering of the pores. This ordering can be seen in the scanning electron microscopy (SEM) picture in Figure 2a, which shows a typical area on the surface with multiple domains of crystalline pores that repeat the orientation of the original latex templates. Both hexagonal (Fig. 2b) and square (Fig. 2c) arrays are observed, the latter much less frequently since these crystals grow only at specific film thicknesses or nucleation conditions.[6] The films in Figures 2b and c correspond to a thickness of two layers of latex particles (~1.1 μm).

Another, even thinner, structure (Fig. 2d) was made by adding less gold than necessary to make an interconnected film. The gold rings probably formed due to the menisci developing around the latex particles in the first layer just before the latex/gold film was completely dry, causing the gold particles to collect around the base of the latex particles, as previously observed with another system.[7] The ring spacing is consistent with the lattice constant of the original latex crystal. To confirm the particulate nature of the gold structures, atomic force microscopy (AFM) imaging (Fig. 2e) was per-

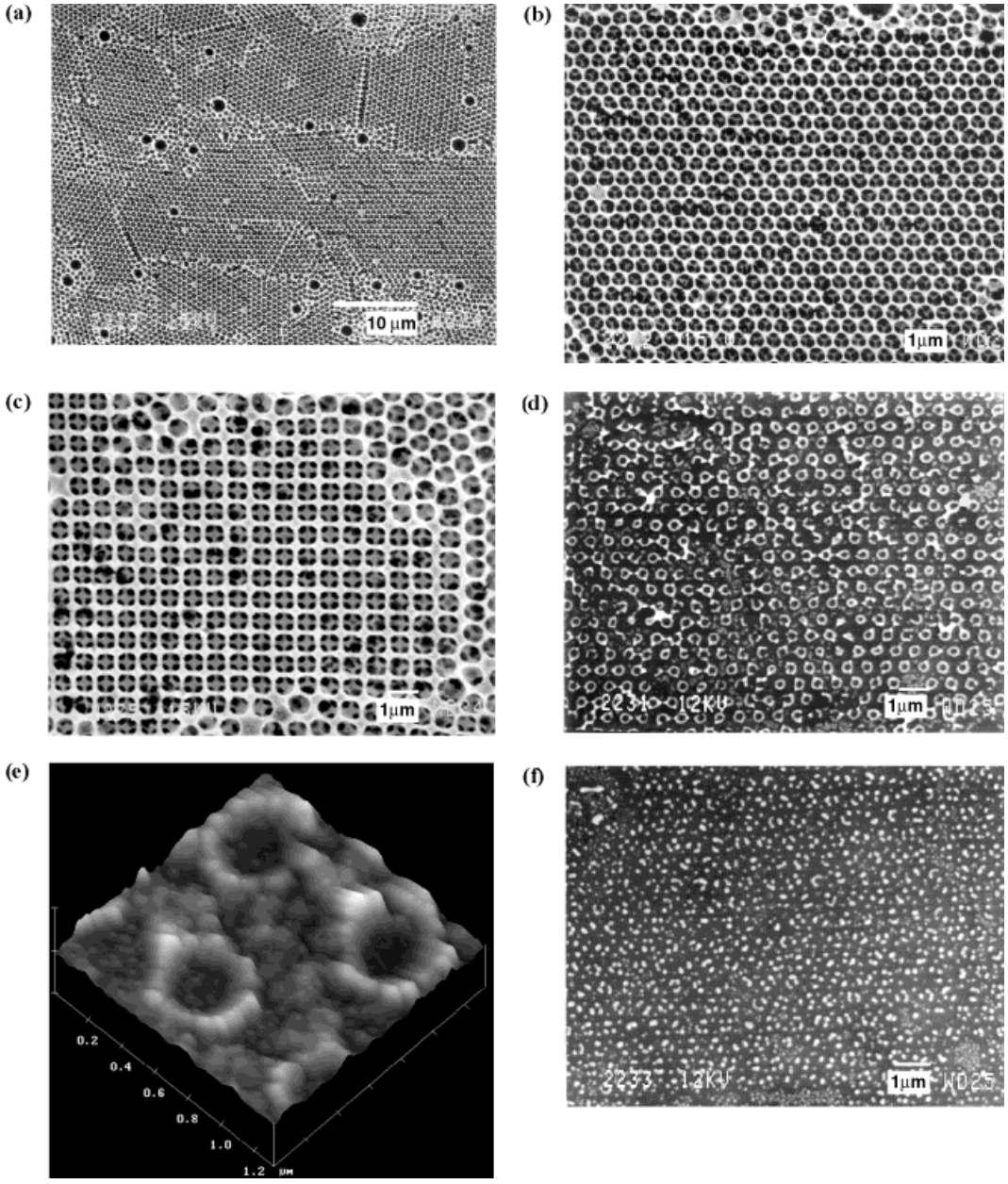

Fig. 2. SEM and AFM images of several porous gold structures. a) SEM image of a hexagonal bilayer that reveals the polycrystalline structure. b) SEM image of a large hexagonal domain at higher magnification. c) SEM image of square bilayer. d) SEM image of a sub-monolayer ring structure. e) AFM image of (d). f) SEM image of (d) after being heated to 500 °C.

  0935-9648/01/0603-0398 $ 17.50+.50/0

formed on a sample similar to that shown in Figure 2d. The individual gold particles can be seen on the glass surface and aggregated together in the gold rings. The nanoparticle framework of the gold structures provides another level of porosity that gives the structures very high surface area. When samples such as that in Figure 2d were heated to ca. 500 °C, the gold particles agglomerated into larger droplets, destroying the original structure while still retaining some degree of long-range order imparted by the colloidal crystal (Fig. 2f).

Structures from gold nanoparticles are of particular optical interest due to their surface plasmon mode, which can easily be characterized by spectroscopy in the visible to infrared (IR) region. The strongest factor affecting the location and width of the surface plasmon mode is the spacing between adjacent gold particles. When gold colloids are aggregated, a new "red-shifted" feature appears in the spectrum,[8] which is likely due to the coupling of the surface plasmons between adjacent particles.

Two interesting effects of significant practical importance that are also likely due to the interacting surface plasmons in metallic films are the surface-enhanced Raman scattering of adsorbed molecules[9] and the exceptional transmission of light through porous metallic films.[10] The physical basis for this connection is that the surface plasmons produce very high electric fields in localized areas (i.e., between neighboring gold nanospheres or in the openings of a porous metallic film). Thin silver films with periodic arrays of pores have been shown to transmit up to twice as much light as actually impinges on the openings, indicating that the high electric fields due to the surface plasmons collect and funnel light through the openings.[11] Such periodic structures have also been shown to enhance the Raman scattering of molecules close to the surface due to these high electric fields.[12]

The infrared-visible (IR-vis) transmission spectra of several different metallic films are shown in Figure 3. Spectrum 1 was obtained with a thin structured sample similar to that shown in Figure 2d, while Spectrum 3 was obtained with a film of gold particles deposited without latex particles, and therefore randomly distributed on the surface. Spectra 2 and 4 are of the structured and unstructured gold particles respectively, after heating to approximately 500 °C. For the structured gold sample before heating (Spectrum 1), a "red-shifted" minimum in the transmission spectrum is observed in the IR region, which is also observed for aggregated colloidal gold in solution.[8] The similarity between the spectra of our structured samples and the spectra of randomly aggregated gold particles indicates that the optical properties of the structured films were determined largely by the close packing of the gold particles. It is also likely that the crystalline ordering of the films, that is, on the order of visible light (630 nm), also contributed to the transmission properties in the visible to IR region. The gold films deposited by the same procedure, but without latex particles (Spectrum 3), show spectra similar to that of unaggregated gold in solution, probably because the gold particles are not close enough together to interact.

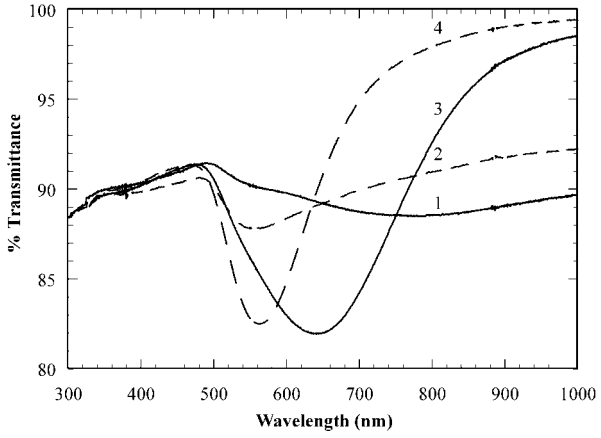

Fig. 3. IR-vis spectroscopy of gold nanoparticles assembled on glass. 1) Structured gold film. 2) Same as (1), but heated to 500 °C. 3) Unstructured gold particles. 4) Same as (3), but heated to 500 °C.

Upon heating of the structured film (Spectrum 2), the broad minimum in the IR region is removed and a sharper peak is seen at the position of the surface plasmon mode. The unstructured film after heating (Spectrum 2) shows a similar surface plasmon mode, but with higher transmission in the IR region than for the structured film. The difference in transmission may be due to the ordered droplets that form after the melting of the structured films (Fig. 2f), which remain close enough to interact.

Since the IR-vis spectra show the presence of collective surface plasmon interactions indicating SERS activity, we characterized the performance of our structures as substrates for Raman spectroscopy (Table 1). We used *trans*-1,2-bis(4-pyridyl)ethylene (BPE) as the model compound. Monolayer

Table 1. Comparison of Raman spectroscopy peak intensities for BPE adsorbed on nanostructured gold surfaces.

Sample	Signal intensity [AU]	
	1019 [cm^{-1}]	1196 [cm^{-1}]
structured monolayer	670	988
unstructured monolayer	316	466
structured monolayer after heating	13	17
structured multilayer	5450	6279
electrochemically roughened	58	70
bulk solid BPE	330	230

structured films (Fig. 2d) yielded twice the Raman signal as for unstructured films, indicating that the structure contributes to the observed enhancement. The importance of the substrate periodicity for the SERS enhancement correlates with the earlier results of others based on periodic microfabricated substrates.[13] The importance of the nanoparticle structure and porosity for the SERS activity is also demonstrated by comparison with the heated substrates (see Fig. 2f), where the activity is almost completely lost (Table 1). This reflects the fact that the larger gold droplets are SERS inactive.

The enhancement of the Raman signal for the multilayer structured films (Fig. 2a–c) was another order of magnitude greater than for the thin structured samples (Fig. 2d). This suggests that the increased amount of gold per scattering cross section provides a significant contribution to the Raman sig-

  0935-9648/01/0603-0399 $ 17.50+.50/0

ADVANCED MATERIALS

nal enhancement. The enhancements shown here for the thick structured samples are an order of magnitude higher than results routinely obtained in the literature,[8] and two orders of magnitude higher than our data with electrochemically roughened substrates (Table 1). Further, our signal-to-noise ratio was better than in previous studies,[8] which allowed a tenfold reduction in the data collection time. Additional details are presented elsewhere.[14]

An important advantage of the methods reported in this paper is that the formation of the structured gold films is relatively insensitive to the number of layers of latex particles. This is in sharp contrast to the 2D metallic films formed by vacuum deposition of metal through a mono- or bi-layer of ordered latex particles, which yields a metallic pattern corresponding to the interstitial void area of the crystal.[15] The formation of the latter materials depends on crystallizing only one or two layers of latex particles, which is challenging in practice, while both of our methods can tolerate latex crystals with a large and variable number of layers of particles. Thus the number of layers in the deposition process need not be precisely controlled. Additionally, our materials are porous on two length scales, and have a high surface area for adsorption, making them attractive for sensing applications.

The materials shown here have interesting optical properties that arise from a combination of the passive structured pores and active surface plasmons in the gold nanoparticles. Such porous metallic films can in principle be used as "enhancing filters" to increase selectively the transmission of some wavelengths of light, while preventing the transmission of others, in masks for sub-wavelength lithography,[10] or as highly absorptive coatings for solar panels. More importantly, we have demonstrated that our samples can find immediate application as SERS substrates of superior quality.[14] Unlike many other proposed applications of porous materials, SERS is tolerant to domain boundaries and crystal defects, which are common in materials formed by colloidal crystal templating and would be difficult to avoid without serious compromises in effort and cost. Our substrates, which are highly porous and possess some degree of three-dimensionality, perform at least as well as their expensive microfabricated analogues. Thus we believe that our thin film deposition method demonstrates the main advantages of colloidal crystal templating, namely the fabrication of advanced structures by simple and inexpensive procedures.

Experimental

Synthesis: Gold nanoparticles (25 nm) were prepared by standard procedures [16] and latex microspheres (630 nm sulfate) were obtained from IDC (Portland, OR). Both types of particles were concentrated by centrifugation at 1600 g for approximately 2 h, yielding 5 wt.-% gold and 20 vol.-% latex solutions. Tween 20 from Sigma (St. Louis, MO) was added to the latex particles before centrifugation to a final concentration of 0.0002 wt.-% to prevent aggregation. In the set-up shown in Figure 1a, the top slide was attached to an electric motor at an angle of ca. 30° relative to the lower slide and could be moved horizontally at a speed of 1–200 μm/s. The gold/latex solutions were mixed in a 9:1 ratio, and 20 μL was dispensed at the angle between the two plates.

The cell for radial deposition of the crystals in Figure 1b used a thin piece (2 mm) of Celerus reinforced fluoroelastomer from W. L. Gore (Newark, DE) to form a deposition chamber with a 6 mm circular opening on a glass slide. To obtain a concave meniscus in the cell, the bottom half of the inner wall of the rubber seal was carved out as shown in Figure 1b. As previously reported [4], this small modification is critical to forming a meniscus that is thinnest in the center and therefore able to nucleate a crystal in the center of the cell. The rubber seal was then placed on a glass slide, and clamped between two steel plates also having a circular opening. About 30 μL of a mixture of latex and gold particles, at approximately the same concentrations as in the previous method, was dispensed into the rubber opening. It was often necessary to wet the sides of the rubber seal with a pipette tip to obtain the proper meniscus. After the sample had dried, the latex template was removed by dipping the substrate in toluene for approximately 15 min.

SEM/AFM Imaging: SEM images were obtained using a JEOL JXA-840 operating at 20 kV. AFM image was obtained by tapping mode in air using a Nanoscope III (DI).

IR-vis Spectroscopy: Transmission spectra were obtained using a PE Lambda 2 UV-vis spectrometer. The samples were fixed at a 20° angle relative to the incident beam to minimize interference with reflected light.

Raman Spectroscopy: A sample of 5 μL of 1 mM BPE (Aldrich, Milwaukee, WI) in methanol was dispensed onto the substrate and allowed to dry. A 785 nm laser operating at 60 mW was focused on a 15 μm diameter spot. The Raman spectrograph system used was a Kaiser Optical Inc. HoloSpec F/1.8 connected to an Olympus BX-60 by a fiber optic cable. The Raman signal was integrated for 10 × 10 s.

Received: October 9, 2000

[1] a) P. Jiang, J. Cizeron, J. F. Bertone, V. L. Colvin, *J. Am. Chem. Soc.* **1999**, *121*, 7957. b) H. W. Yan, C. F. Blanford, B. T. Holland, M. Parent, W. H. Smyrl, A. Stein, *Adv. Mater.* **1999**, *11*, 1003. c) G. L. Egan, J.-S. Yu, C. H. Kim, S. J. Lee, R. E. Schaak, T. E. Mallouk, *Adv. Mater.* **2000**, *12*, 1040.

[2] a) J. Wijnhoven, S. J. M. Zevenhuizen, M. A. Hendriks, D. Vanmaekelbergh, J. J. Kelly, W. L. Vos, *Adv. Mater.* **2000**, *12*, 888. b) L. B. Xu, W. L. L. Zhou, C. Frommen, R. H. Baughman, A. A. Zakhidov, L. Malkinski, J. Q. Wang, J. B. Wiley, *Chem. Commun.* **2000**, 997.

[3] O. D. Velev, P. M. Tessier, A. M. Lenhoff, E. W. Kaler, *Nature* **1999**, *401*, 548.

[4] a) N. D. Denkov, O. D. Velev, P. A. Kralchevsky, I. B. Ivanov, H. Yoshimura, K. Nagayama, *Langmuir* **1992**, *8*, 3183. b) N. D. Denkov, O. D. Velev, P. A. Kralchevsky, I. B. Ivanov, H. Yoshimura, K. Nagayama, *Nature* **1993**, *361*, 26.

[5] A. S. Dimitrov, K. Nagayama, *Langmuir* **1996**, *12*, 1303.

[6] P. Pieranski, *Contemp. Phys.* **1983**, *24*, 25.

[7] J. Boneberg, F. Burmeister, C. Schafle, P. Leiderer, D. Reim, A. Fery, S. Herminghaus, *Langmuir* **1997**, *13*, 7080.

[8] K. C. Graber, R. G. Freeman, M. B. Hommer, M. J. Natan, *Anal. Chem.* **1995**, *67*, 735.

[9] J. A. Creighton, C. G. Blatchford, M. G. Albrecht, *J. Chem. Soc., Faraday Trans. 2* **1979**, *75*, 790.

[10] T. W. Ebbesen, H. J. Lezec, H. F. Ghaemi, T. Thio, P. A. Wolff, *Nature* **1998**, *391*, 667.

[11] J. Pendry, *Science* **1999**, *285*, 1687.

[12] F. J. Garcia, J. B. Pendry, *Phys. Rev. Lett.* **1996**, *77*, 1163.

[13] M. Kahl, E. Voges, S. Kostrewa, C. Viets, W. Hill, *Sens. Actuators A* **1998**, *51*, 285.

[14] P. M. Tessier, O. D. Velev, A. T. Kalambur, J. F. Rabolt, A. M. Lenhoff, E. W. Kaler, *J. Am. Chem. Soc.* **2000**, *122*, 9554.

[15] J. C. Hulteen, R. P. Van Duyne, *J. Vac. Sci. Technol. A* **1995**, *13*, 1553.

[16] a) J. W. Slot, H. J. Geuze, *J. Cell. Biol.* **1981**, *90*, 533. b) J. W. Slot, H. J. Geuze, *Eur. J. Cell. Biol.* **1985**, *38*, 87.

  0935-9648/01/0603-0400 $ 17.50+.50/0